Supporting Information

A green and efficient strategy for fabricating supercapacitor electrodes using mechanochemically synthesised Cu-HHTP MOF

Danilo Marchetti, [a] Silvio Scaravonati, [b] Goulielmina Anyfanti, [c] Lucrezia Aversa, [d] Roberto Verucchi, [d] Mauro Riccò, [b] Chiara Massera, [a] Mauro Gemmi, [c] Daniele Pontiroli [b,*] and Alessandro Pedrini [a,*]

a Department of Chemistry, Life Sciences and Environmental Sustainability, INSTM UdR Parma, University of Parma, Parco Area delle Scienze 17/A, Parma, Italy.

b Department of Mathematical, Physical and Computer Sciences, University of Parma, Parco Area delle Scienze 7/A, 43124, Parma, Italy.

c Center for Materials Interfaces, Electron Crystallography, Istituto Italiano di Tecnologia, Viale Rinaldo Piaggio 34, 56025 Pontedera, Italy.

d Institute of Materials for Electronics and Magnetism, IMEM-CNR, FBK Trento unit c/o Fondazione Bruno Kessler, Via alla Cascata 56/C, Trento, 38123, Italy.

E-mail: daniele.pontiroli@unipr.it; alessandro.pedrini@unipr.it

Table of contents

1. Synthesis of Cu-HHTP MOF

General mechanochemical method

The mechanochemical synthesis was carried out in a 5 mL agate jar, with two 5 mm agate spheres. The reagents were placed into the jar, and the grinding was performed at 20 Hz for 30 minutes.

In those reactions carried out through a liquid-assisted grinding (LAG), the amount of liquid additive was defined through the following relation:

$$\eta = \frac{Additive\ volume\ (\mu L)}{Total\ mass\ solid\ reagent\ (mg)}$$

where η corresponds to the liquid-to-solid ratio, also described as LAG parameter, and it is defined as the ratio between the ηL of the liquid additive and the total mass of the solid reagents expressed in mg.

Table S1. Experimental details for the mechanochemical reactions conducted using different liquid-to-solid ratios (η).

Sample	$Cu(OAc)_2 \cdot H_2O$ mass (mg)	$Cu(OAc)_2 \cdot H_2O$ moles (mmol)	HHTP mass (mg)	HHTP moles (mmol)	M/L molar rate	Additive volume (μL)	η
0	38.0	0.190	32.3	0.0995	1.9	0	0
1	36.7	0.184	30.0	0.0925	2.0	70	1.0
2	38.5	0.193	29.9	0.0924	2.1	140	2.0

Table S2. Experimental details for the mechanochemical reactions conducted using different metal salts.

Sample	Metal salt mass (mg)	Metal Salt moles (mmol)	HHTP mass (mg)	HHTP moles (mmol)	M/L molar rate	Additive volume (μL)	η
$Cu(OAc)_2 \cdot H_2O$	38.6	0.193	31.5	0.0973	1.9	71	1.0
$CuSO_4 \cdot 5H_2O$	21.4	0.0856	13.5	0.0417	2.1	35	1.0

Table S3. Experimental details for the mechanochemical reactions conducted using different liquid additives, in which, starting from distilled water, the AcOH concentration was progressively increased.

AcOH (% v/v)	$Cu(OAc)_2 \cdot H_2O$ mass (mg)	$Cu(OAc)_2 \cdot H_2O$ moles (mmol)	HHTP mass (mg)	HHTP moles (mmol)	M/L molar rate	Additive volume (μL)	η
0	39.3	0.197	31.55	0.0973	2.0	70	1.0
5	37.9	0.190	31.11	0.0959	2.0	70	1.0
20	38.5	0.193	32.75	0.101	1.9	70	1.0
50	38.5	0.193	30.75	0.0948	2.0	70	1.0
100	35.7	0.179	30.52	0.0941	1.9	70	1.0

2. Structural Characterization: Powder X-ray diffraction (PXRD) and 3D Electron Diffraction (3D ED)

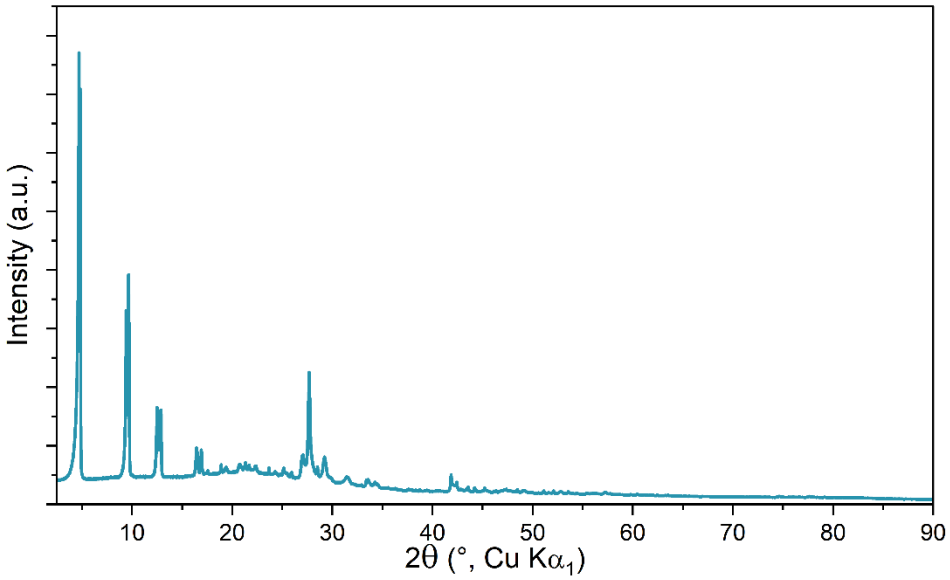

Fig. S1 PXRD profile of the **Cu-HHTP(S)** batch employed in the 3D ED characterisation.

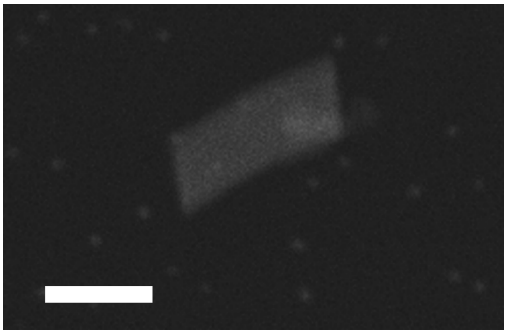

Figure S2. HAADF-STEM image of a **Cu-HHTP** MOF nanocrystal used for the 3D ED data collection. The scale bar corresponds to 200 nm.

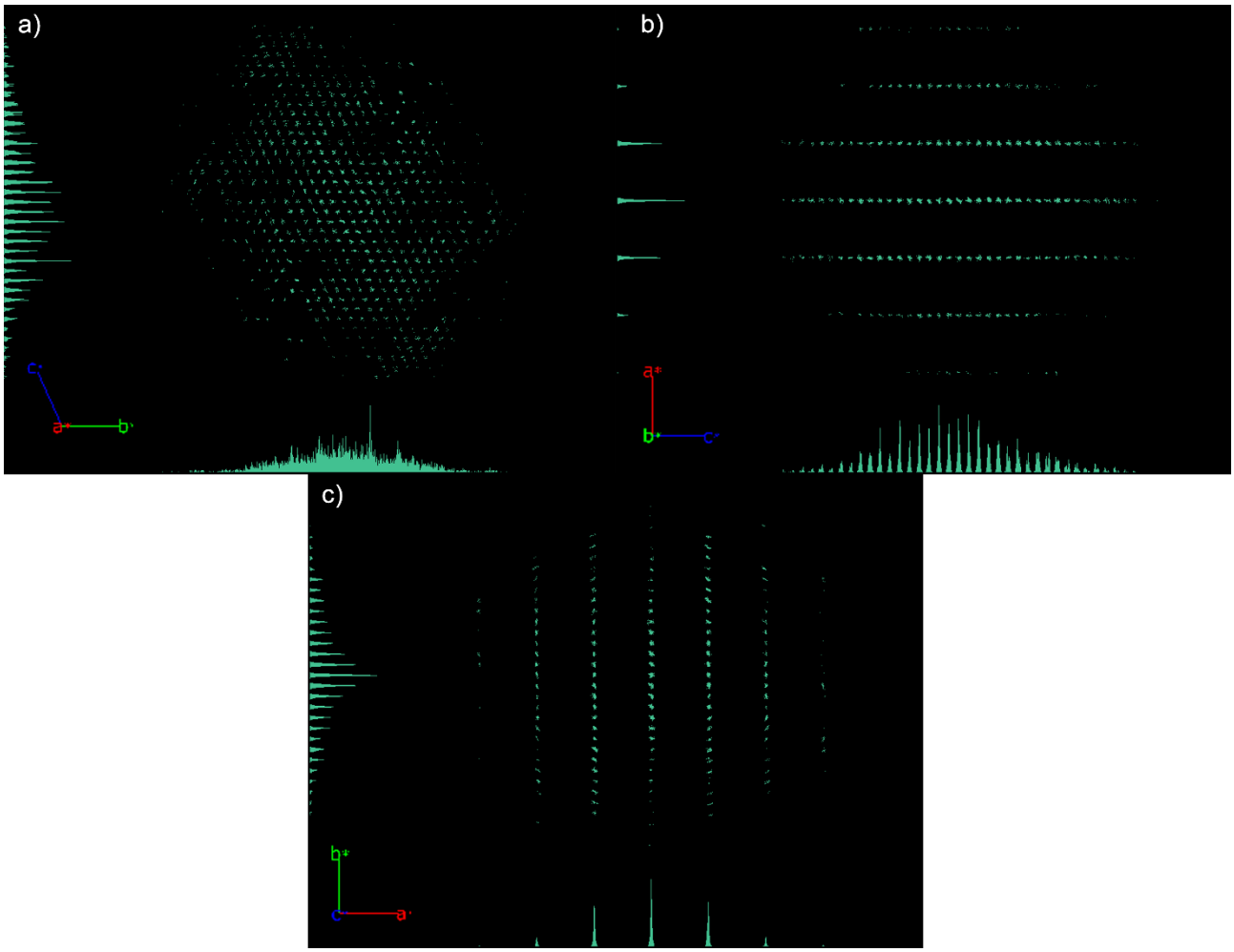

Figure S3. Reciprocal space reconstruction **of Cu-HHTP** obtained with PETS2 from the 3D ED data set. The view has been oriented along the a^*-axis (a), b^*-axis (b), and c^*-axis (c).

Table S4 Crystal data and structure refinement information for **Cu-HHTP**.

Compound	**Cu-HHTP**
Empirical formula	$C_{36}H_{12}Cu_3O_{12}\cdot 6(H_2O)$
Formula weight	827.11
Crystal System	Triclinic
Space Group	$P\bar{1}$
a/Å	3.590(2)
b/Å	19.61(2)
c/Å	20.698(17)
α/°	63.61(8)
β/°	89.91(5)
γ/°	88.71(7)
V/Å^3	1305(2)
Z	1
ρ /g cm^{-3}	1.052
Total reflections	5708
Unique reflections (R_{int})	2170 (0.1808)
Data/retraints/parameters	2170/62/106
GOF on F^{2a}	1.032
R indexes [I>=2σ (I)]^b	R_1 = 0.2035, wR_2 = 0.4932
R indexes [all data]	R_1 = 0.2580, wR_2 = 0.5637
Largest diff. peak and hole (eÅ^{-3})	0.33/-0.23

[a]Goodness-of-fit S = [Σw(F$_o^2$-F$_c^2$)^2/ (n-p)]1/2, where n is the number of reflections and p the number of parameters.

[b]$R_1 = \Sigma \| F_o | - | F_c \| / \Sigma | F_o |$, $wR_2 = [\Sigma[w(F_o^2-F_c^2)^2]/\Sigma[w(F_o^2)^2]]^{1/2}$.

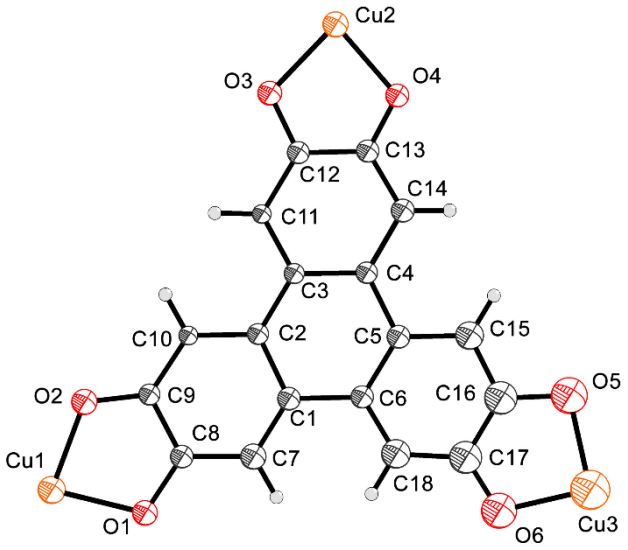

Fig. S4 Ortep view of the asymmetric unit of **Cu-HHTP** with labelling scheme and ellipsoids at the 30% probability level.

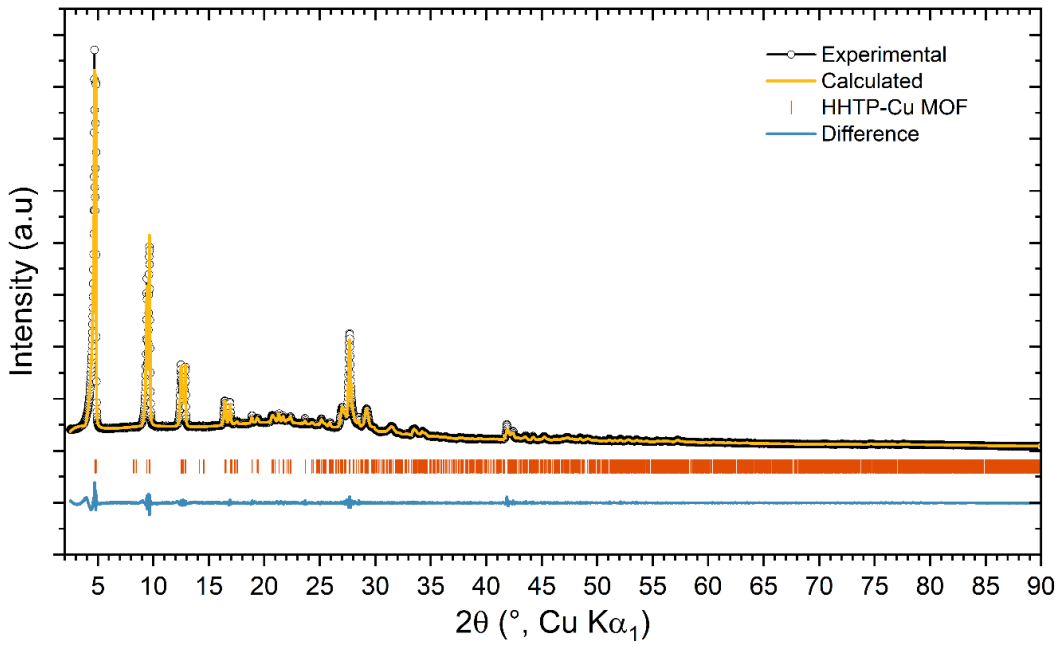

Fig. S5 Profile fit from Pawley refinement carried out on the **Cu-HHTP(S)** batch employed in the 3D ED characterisation. The refinement converged to R_p = 1.88 % and R_{wp} = 2.80 %.

Table S5. Comparison between the unit cell parameters obtained from the PXRD and the 3D ED data for **Cu-HHTP(S)**

	PXRD	**3D ED**
a/Å	3.61054(2)	3.590(2)
b/Å	20.989(1)	19.61(2)
c/Å	21.425(1)	20.698(17)
α/°	61.911(5)	63.61(8)
β/°	90.11(2)	89.91(5)
γ/°	85.99(1)	88.71(7)

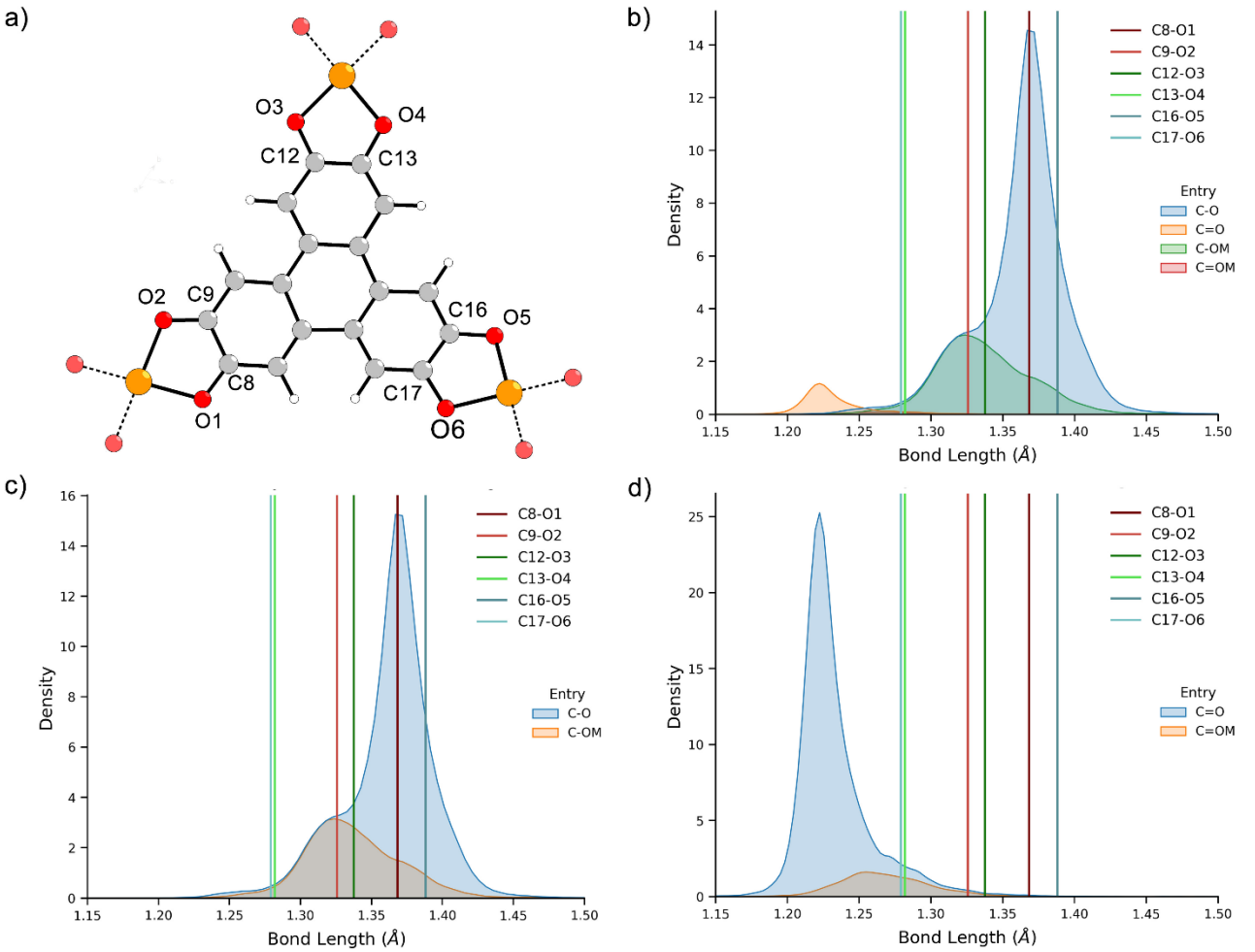

Fig. S6 Schematic representation of the repeating units of **Cu-HHTP** MOF, in which the atoms involved in the C-O bonds have been labelled. (a) Kernel density estimation from the covalent bond distances between C and O, retrieved from the CSD database (version 5.45). The research has been conducted by considering the C···O contacts in systems in which the C atom is part of a 6-membered ring close to planarity (b). Moreover, the contacts have been filtered by considering single (c) and double bonds (d), and with or without the presence of a metal centre close to the oxygen atom.

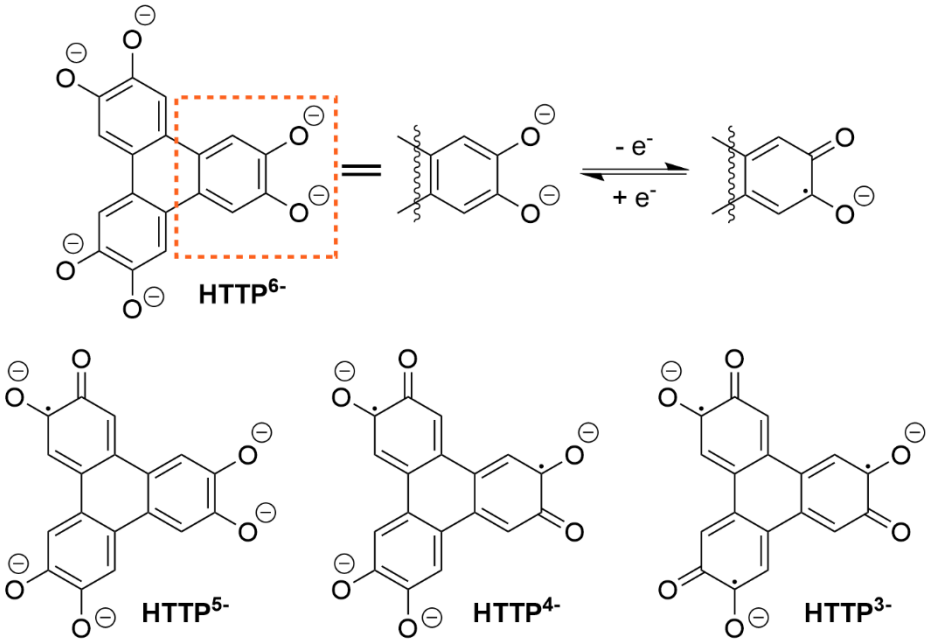

Fig. S7 Schematic representation of the redox behaviour of the $HHTP^{6-}$ molecule followed by its possible oxidation state.

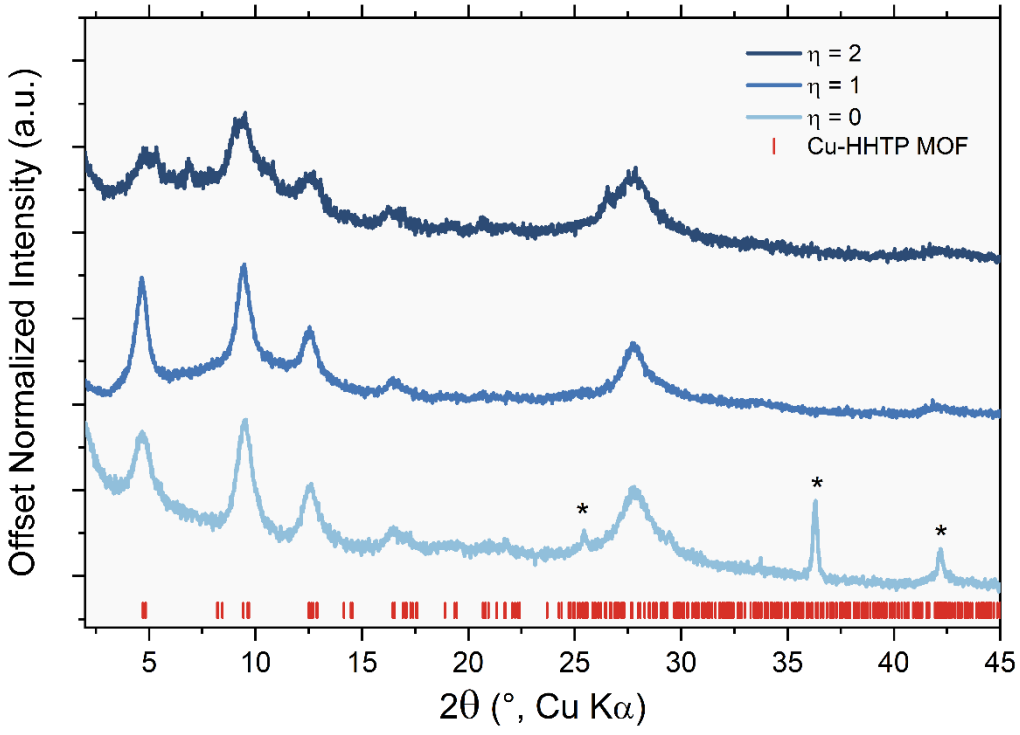

Fig. S8 PXRD profile of the mechanochemical products synthesised using different liquid-to-solid ratios (η). The black stars highlight the presence of a spurious crystalline phase.

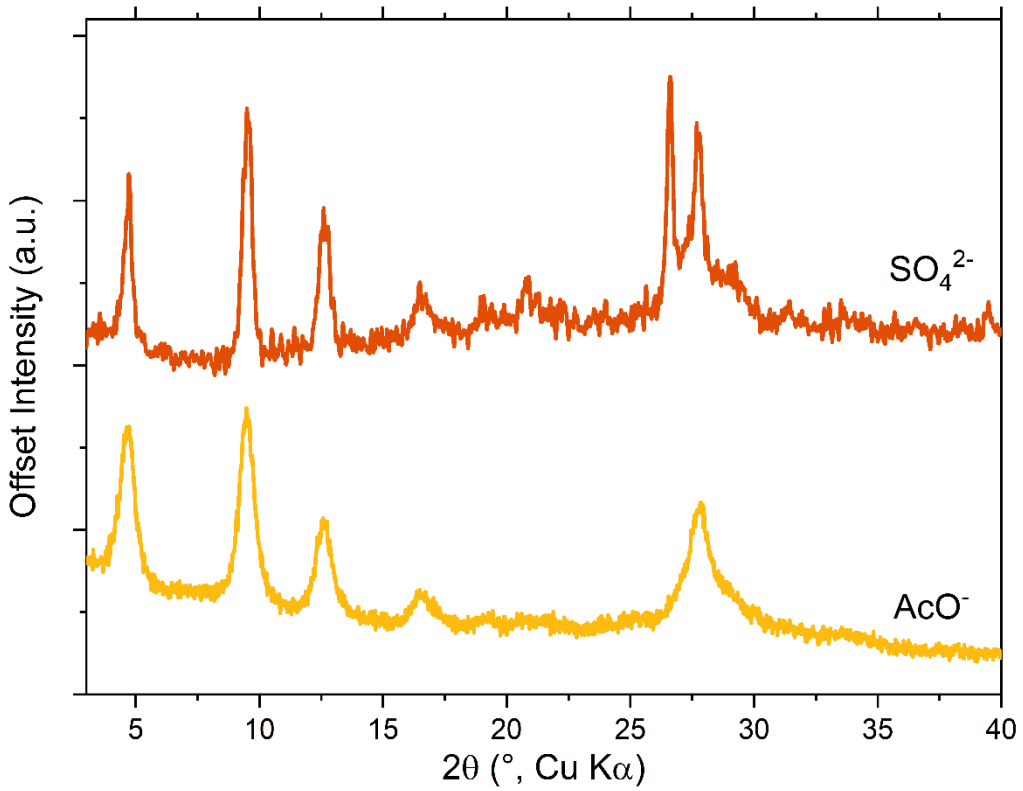

Fig. S9 PXRD profile comparison of the mechanochemical products synthesised using $CuSO_4 \cdot 5H_2O$ or $Cu(OAc)_2 \cdot H_2O$ as reagent, respectively.

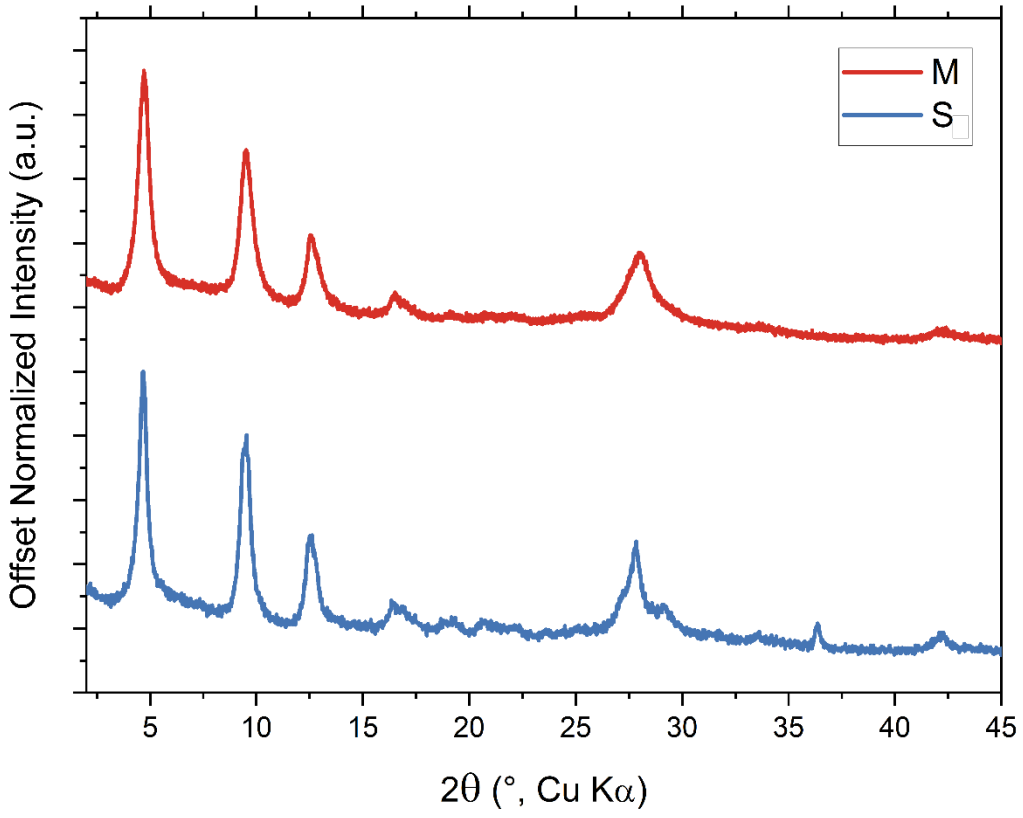

Fig. S10. PXRD profile comparison of the mechanochemical product **Cu-HHTP(M)** and solvothermal **Cu-HHTP(S)**, both synthesised using $Cu(OAc)_2 \cdot H_2O$ as metal salt.

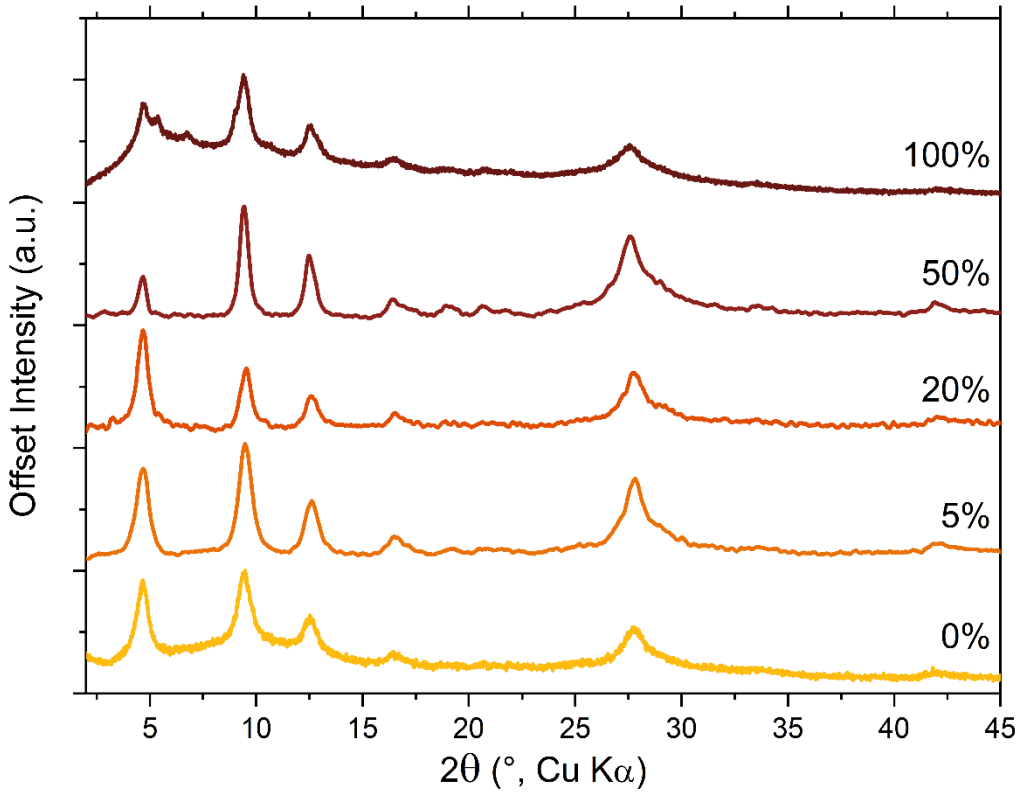

Fig. S11. PXRD profile comparison of the mechanochemical products synthesised employing different concentrations of AcOH in the liquid additive.

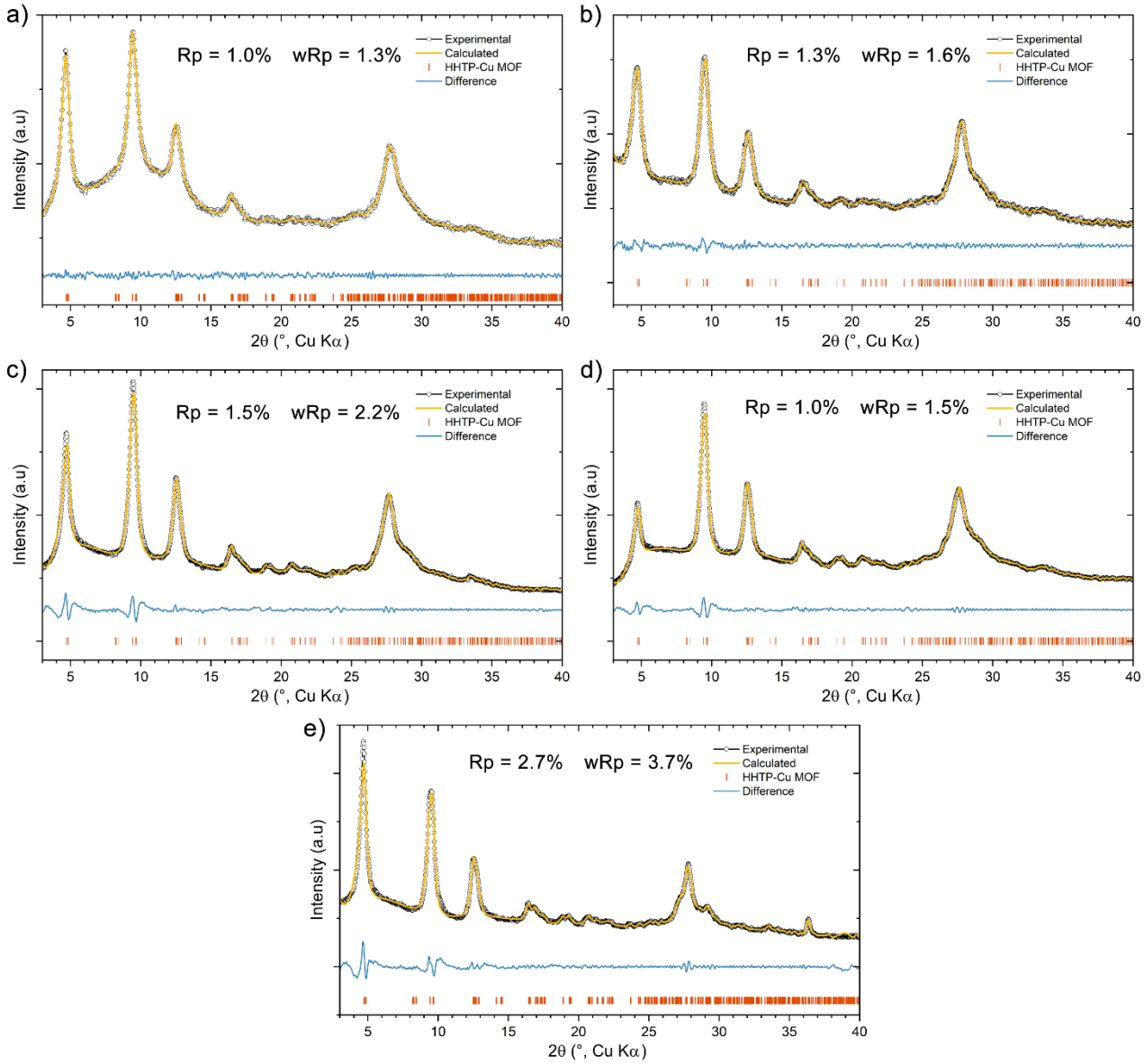

Fig. S12. Peak profile fit from Pawley refinement carried out keeping fixed the instrumental and lattice parameters and refining only the Lorentzian broadening, carried out on: (a) **Cu-HHTP(M)** 0% AcOH, (b) **Cu-HHTP(M)** 5% AcOH, (c) **Cu-HHTP(M)** 20% AcOH, (d) **Cu-HHTP(M)** 50% AcOH, and (e) **Cu-HHTP(S)**.

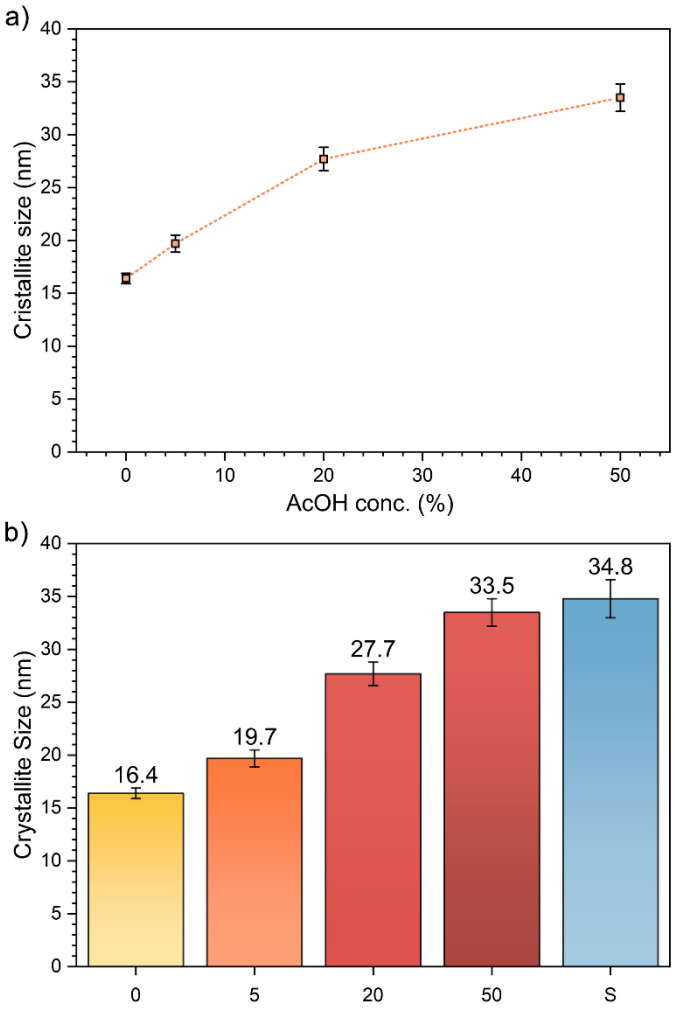

Fig. S13. Plot of the crystallite size values estimated from the Lorentzian broadening component of the PXRD peak profiles for the mechanochemical products (a) and their comparison with the solvothermal analogous S (b).

3. Thermogravimetric analysis (TGA)

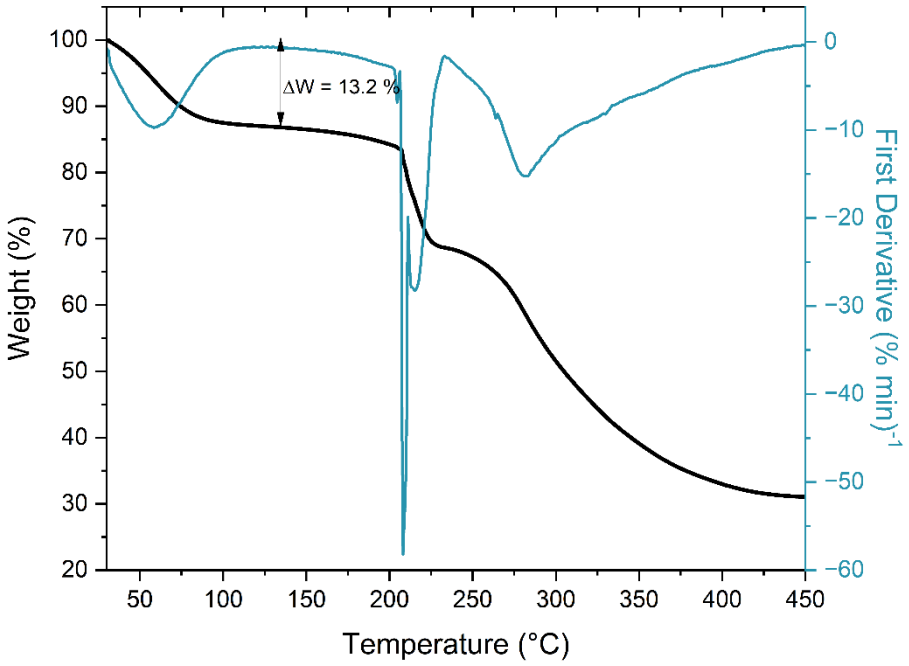

Fig. S14. Thermogravimetric path recorded on **Cu-HHTP(S)**. From the measured weight loss of 13.2% 7 molecules of water per formula unit have been estimated.

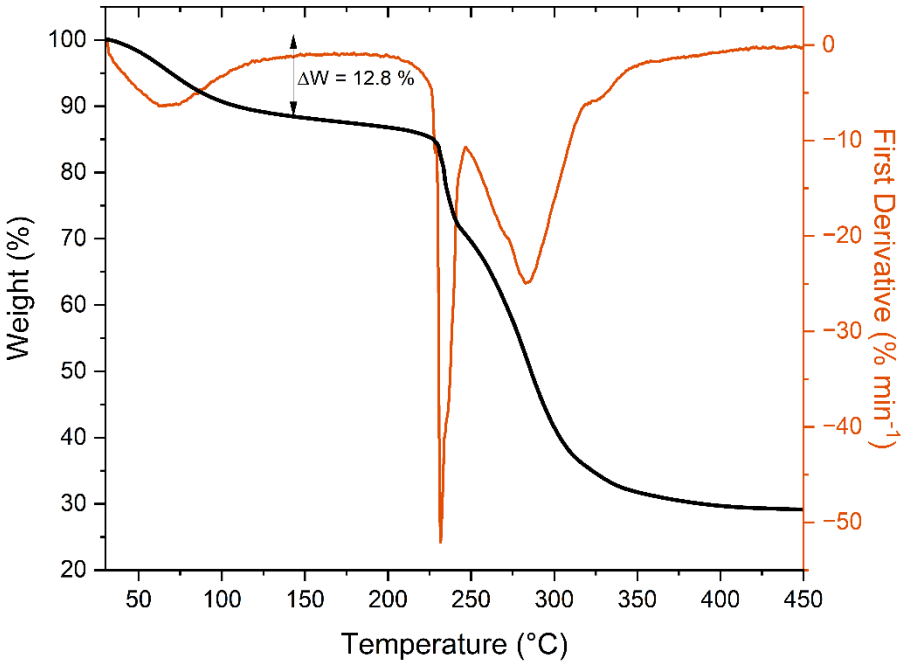

Fig. S15. Thermogravimetric path recorded on **Cu-HHTP(M)**. From the measured weight loss of 12.8% 6.8 molecules of water per formula unit have been estimated.

4. Scanning Electron Microscopy (SEM)

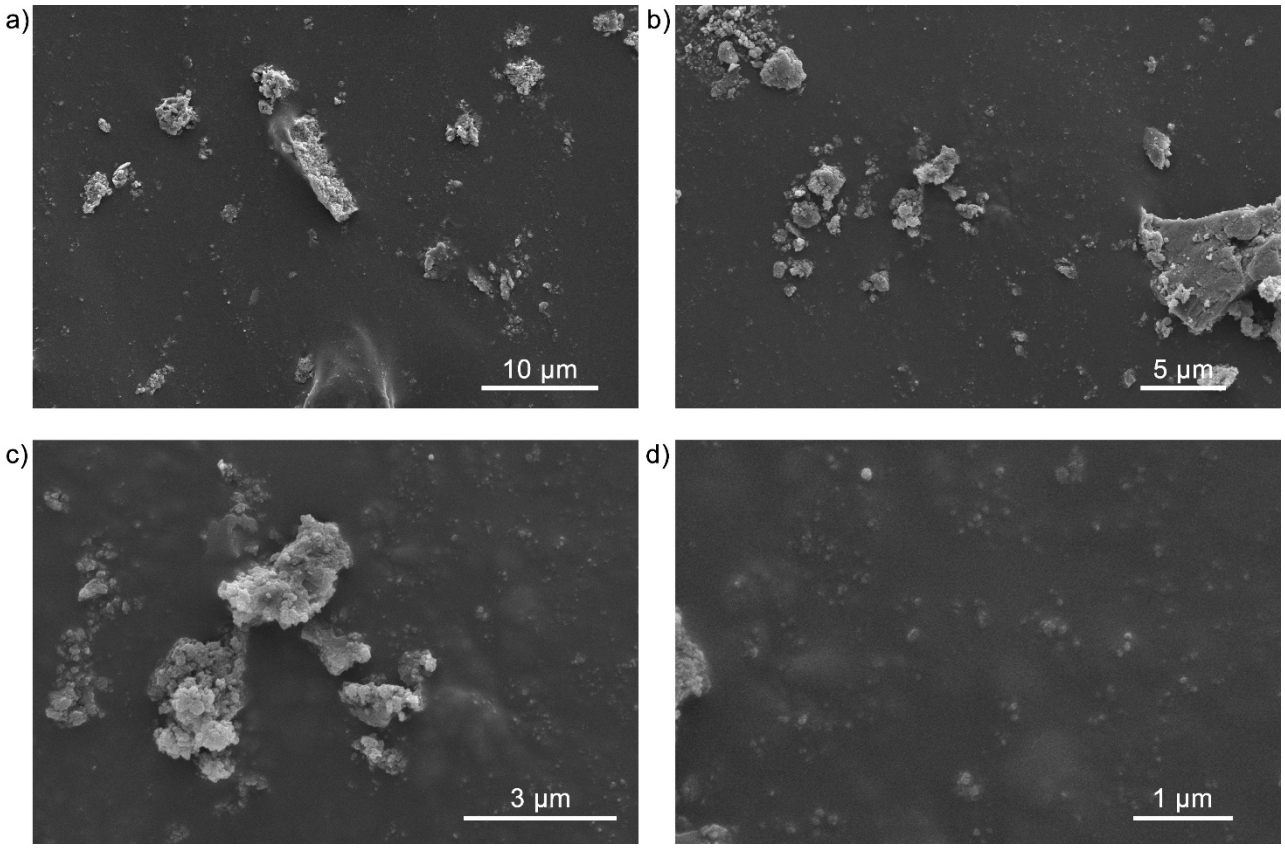

Fig. S16. SEM images of **Cu-HHTP(M)**.

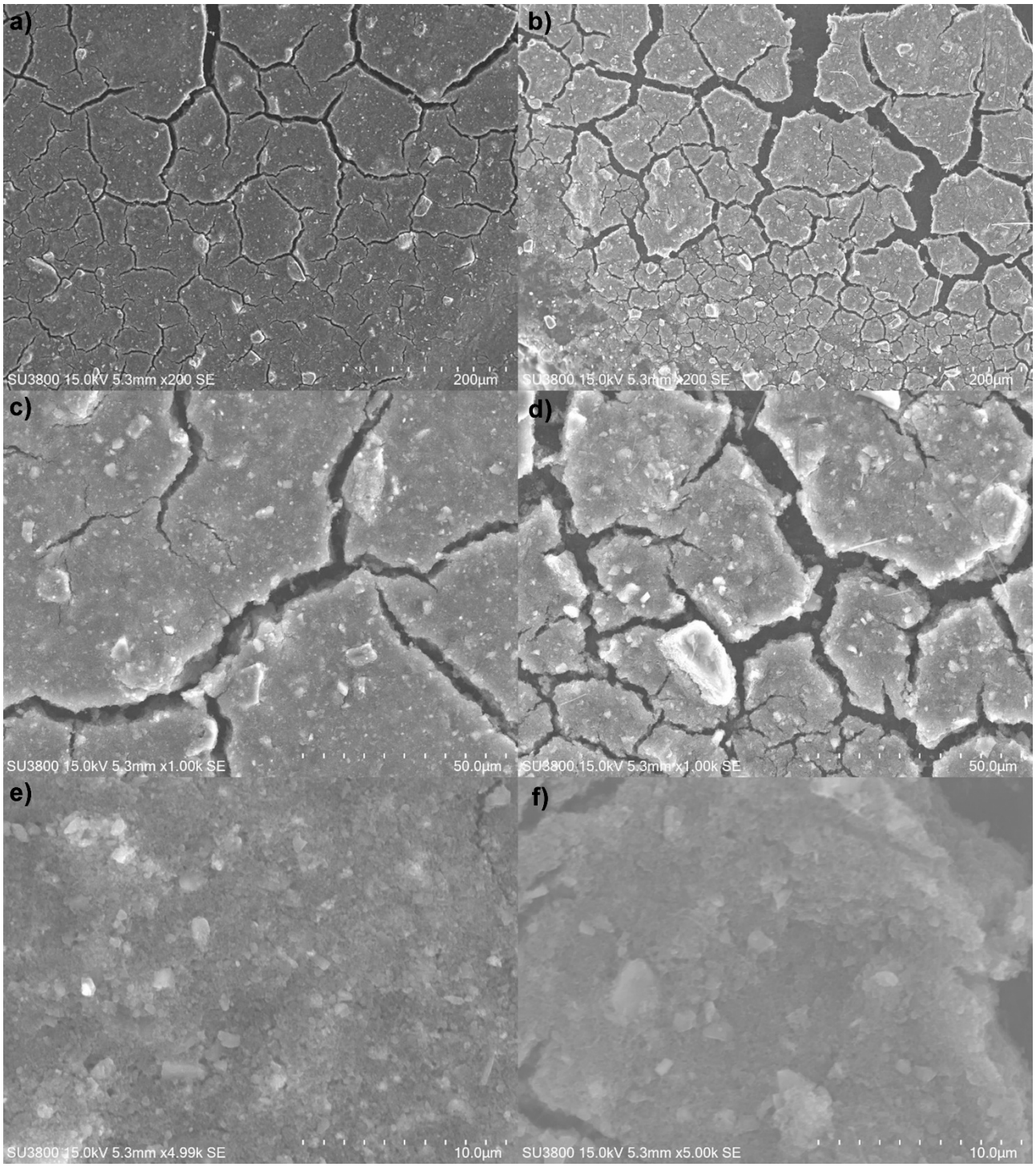

Fig. S17. SEM of **Cu-HHTP(S)** uncycled electrode (a, c, e) and cycled negative electrode (b, d, f) at different magnification. Needle-like structures are glass microfiber separator residues.

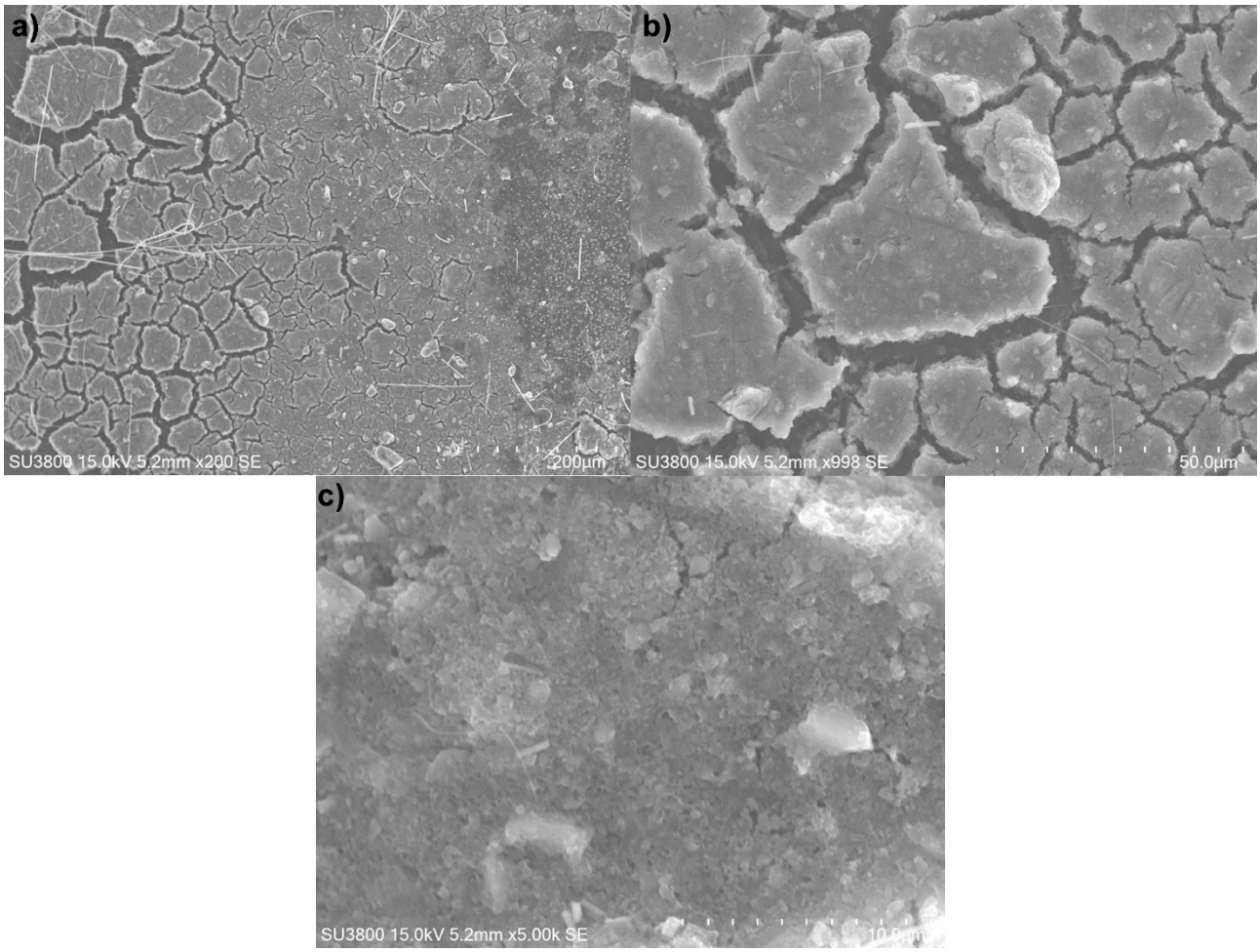

Fig. S18. SEM of **Cu-HHTP(S)** cycled positive electrode at different magnification (a, b, c). Needle-like structures are glass microfiber separator residues.

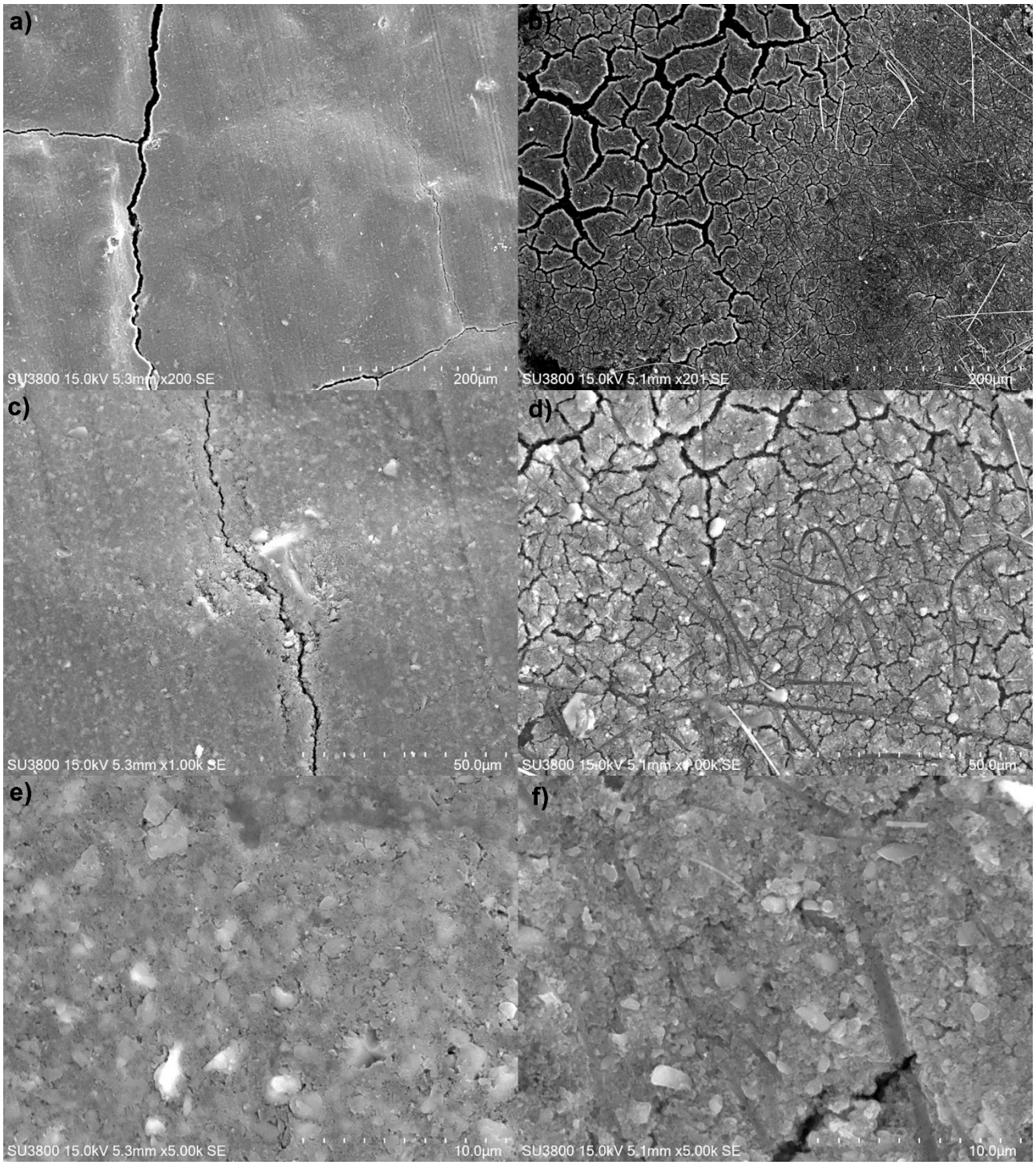

Fig. S19. SEM of **Cu-HHTP(M)** uncycled electrode (a, c, e) and cycled negative electrode (b, d, f) at different magnification. Needle-like structures are glass microfiber separator residues.

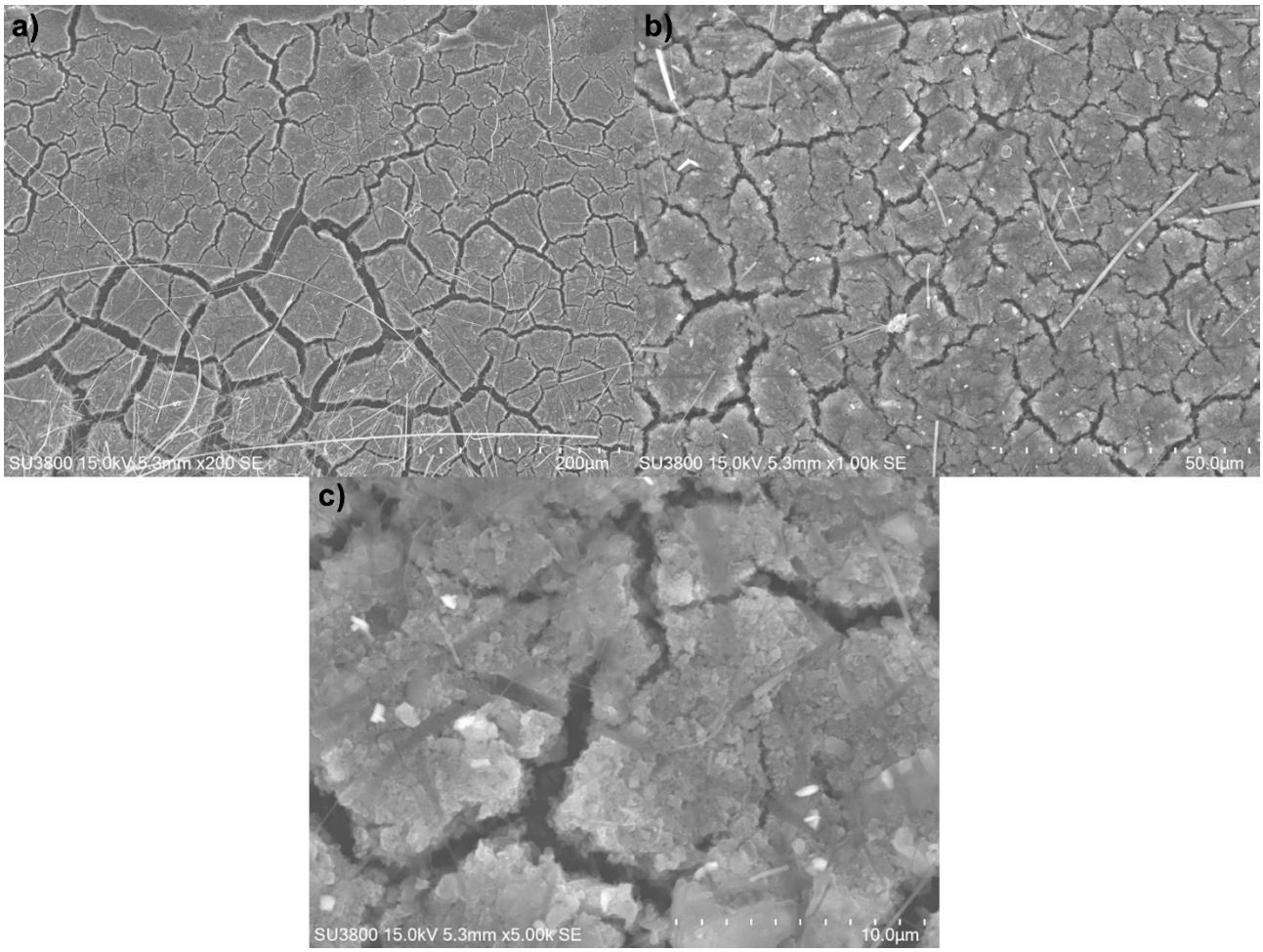

Fig. S20. SEM of **Cu-HHTP(M)** cycled positive electrode (a, b, c) at different magnification. Needle-like structures are glass microfiber separator residues.

5. Gas Sorption analysis

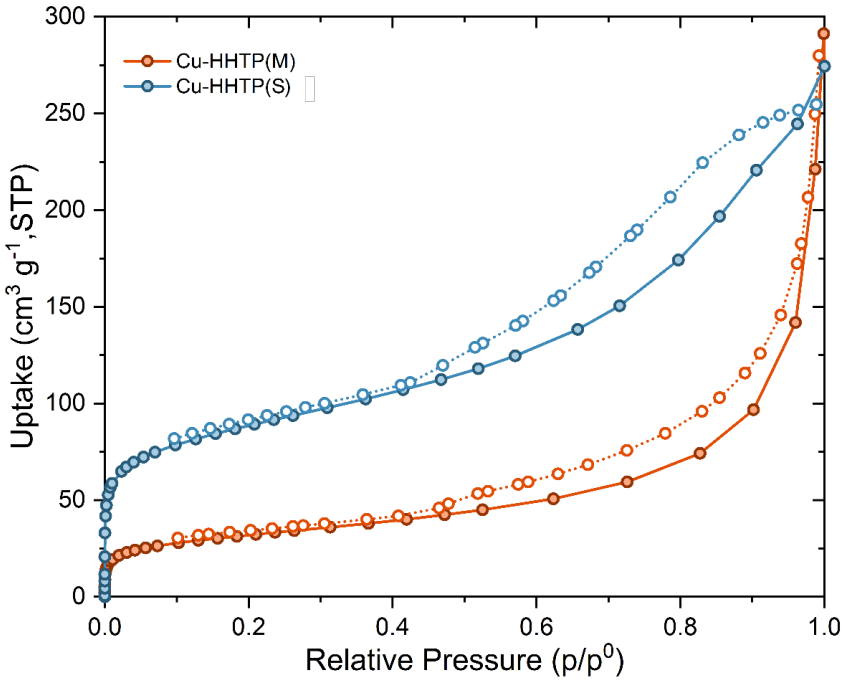

Fig. S21. Nitrogen adsorption isotherm of **Cu-HHTP** MOF obtained through solvothermal (S) and mechanochemical (M) synthesis.

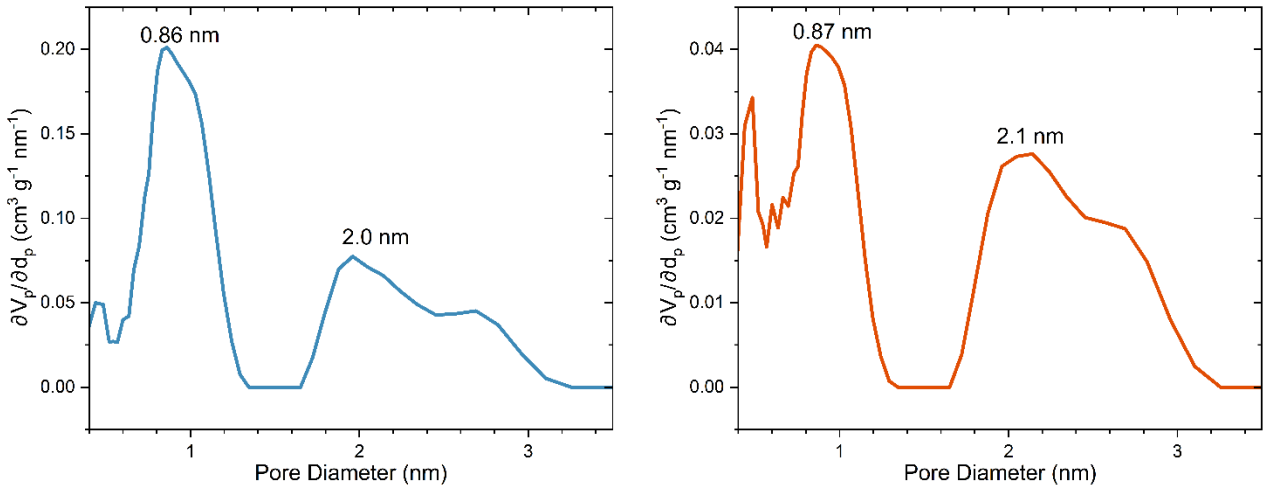

Fig. S22. Pore size distribution plot of (a) **Cu-HHTP(S)** and (b) **Cu-HHTP(M)**.

Table S6. Textural parameters obtained from N_2 adsorption isotherms at 77K for **Cu-HHTP(M)** and **Cu-HHTP(S)**.

	M	**S**
SSA_{BET} (m^2 g^{-1})	114	317
$SSA_{Langmuir}$ (m^2 g^{-1})	140	387
Pore Volume (cm^3 g^{-1})	0.40	0.49
Peak pore size (nm)	0.87, 2.1	0.86, 2.0

6. X-ray Photoelectron Spectroscopy (XPS)

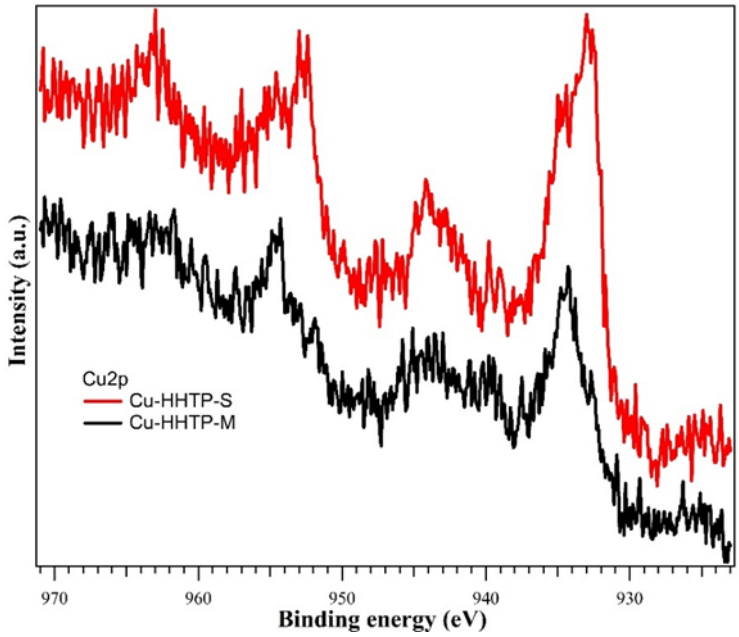

Fig. S23. Low resolution spectra of the Cu2p core level region for **Cu-HHTP(S)** and **Cu-HHTP(M)**. Spectra are not background subtracted.

Table S7. XPS analysis of **Cu-HHTP(S)** and **Cu-HHTP(M)** for all core levels. The binding energy (BE) and percentage of the total peak area for each component are shown.

		Cu-HHTP(S)		Cu-HHTP(M)	
Core level	**Component**	**BE (eV)**	**% on total peak area**	**BE (eV)**	**% on total peak area**
Cu2p 3/2	Cu(0)	932.67	17.6		
	Cu(I)			932.16	8.6
	Cu(II)	934.41	82.4	934.59	91.4
C1s	C1s C-C sp^2	284.20	42.8	284.26	55.5
	C1s C-O	285.95	22.1	285.89	15.3
	C1s C=O	288.03	18.8	288.11	16.6
	C1s C-C sp^3	285.40	16.3	285.46	12.5
O1s	O1s C-OH aromatic	533.39	26.8	533.00	26.9
	O1s C=O aromatic	532.26	23.1	532.33	18.0
	O1s O-Cu	531.20	50.1	531.14	55.1

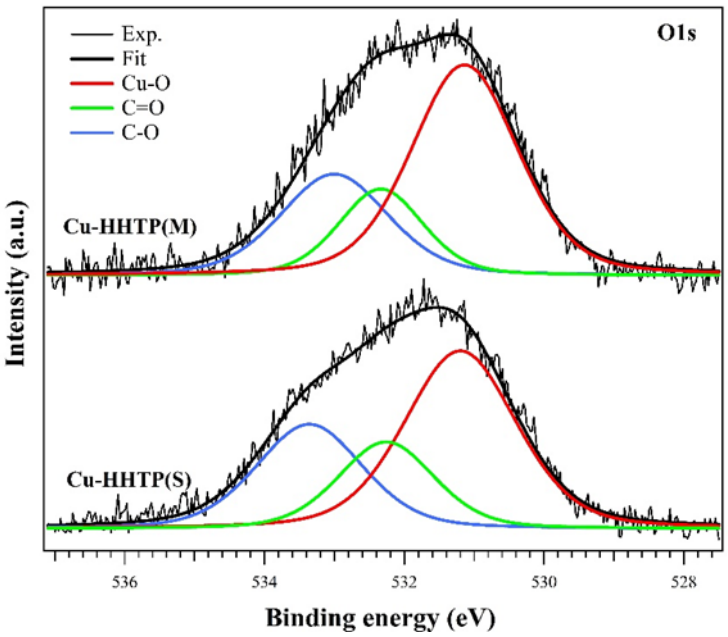

Fig. S24. O1s core level deconvolution for **Cu-HHTP(S)** and **Cu-HHTP(M)**. Spectra are background subtracted. The attribution of each component is shown in the legend.

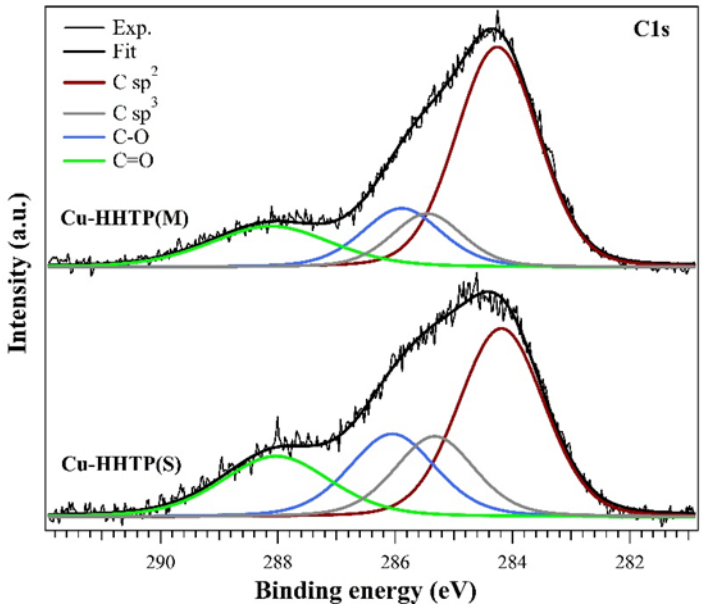

Fig. S25. O1s core level deconvolution for **Cu-HHTP(S)** and **Cu-HHTP(M)**. Spectra are background subtracted. The attribution of each component is shown in the legend.

7. Electrochemical Characterisation

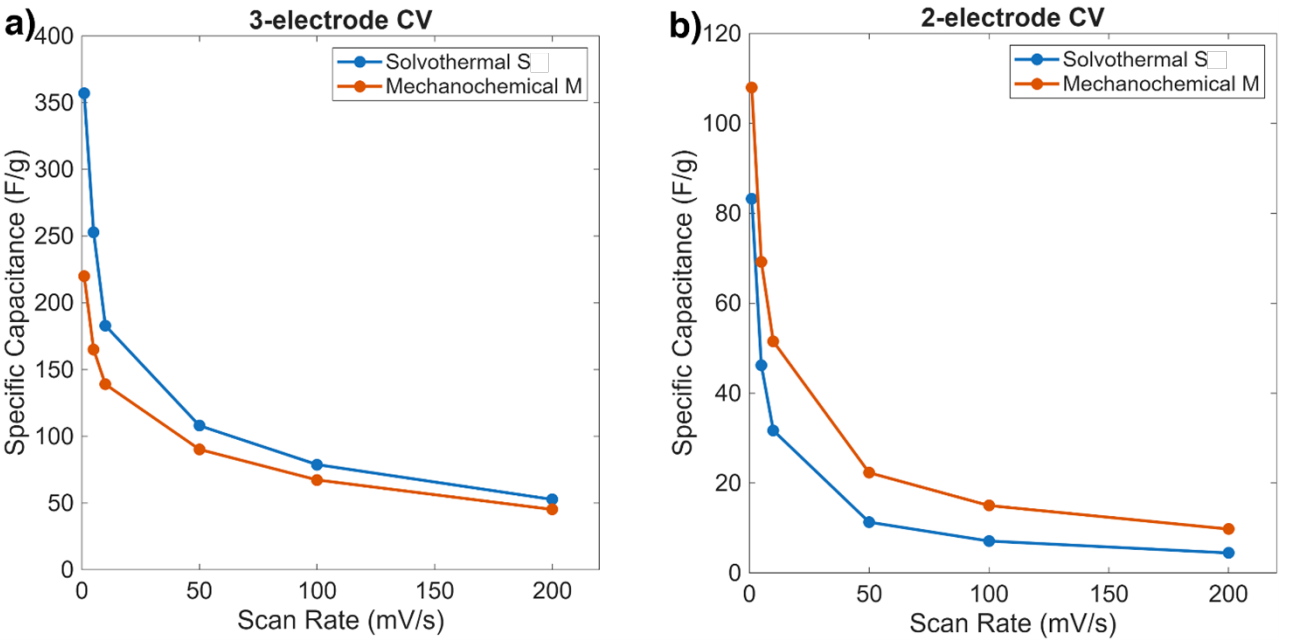

Fig. S26. Specific ~~capacity~~ capacitance of **Cu-HHTP(S)** and **Cu-HHTP(M)** electrodes calculated from a) 3-electrode CV and b) 2-electrode CV

Table S8. b-values calculated from CV at different scan rates

		Cu-HHTP(S)	Cu-HHTP(M)
anodic	**Potential (V)**	0.04	0
	b-value	0.53 ± 0.14	0.68 ± 0.08
	R-square (%)	96.2	99.3
cathodic	**Potential (V)**	-0.11	-0.08
	b-value	0.60 ± 0.08	0.83 ± 0.13
	R-square (%)	99.1	98.7

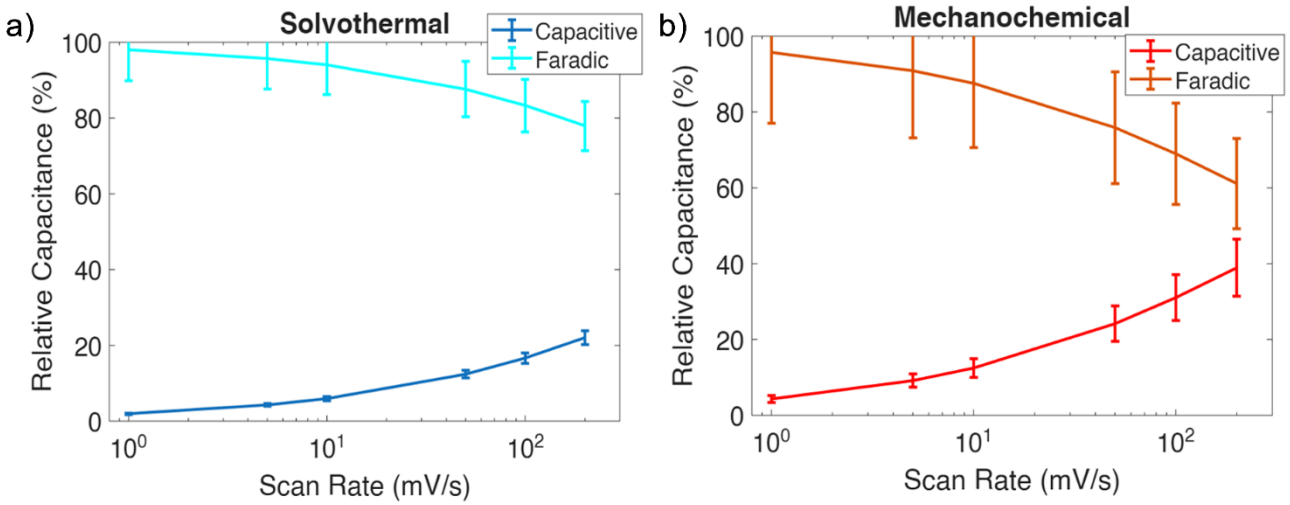

Fig. S27. EDLC and Redox contribution for (a) **HHTP-Cu(S)** and (b) **HHTP-Cu (M)**.

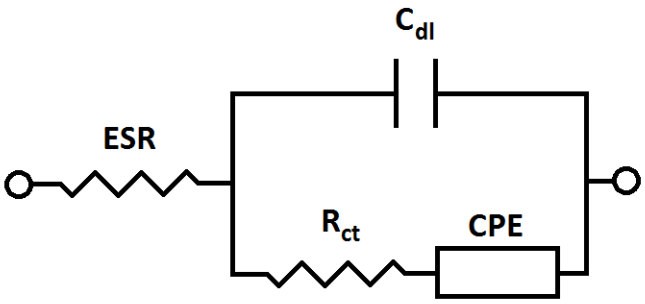

Fig. S28. Model employed for the analysis of the EIS spectra.

ESR is the equivalent series resistance, C_{dl} is the double layer capacitance, R_{ct} is the charge transfer resistance, and CPE is a constant phase element which is the result of the frequency dependence of ion diffusion in the electrolyte, whose impedance is given by:

$$Z_{CPE} = \frac{1}{A_0(j\omega)^{\gamma}}$$

Table S9. Fit parameters for EIS on symmetrical devices with **Cu-HHTP(S)** and **Cu-HHTP(M)**-based electrodes.

	Cu-HHTP(S)	**Cu-HHTP(M)**
ESR (Ω)	2,72 ± 0,1	3,9 ± 0,1
C_{dl} (F)	(2,8 ± 0,2) · 10^{-6}	(2,5 ± 0,1) · 10^{-6}
R_{ct} (Ω)	5,1 ± 0,8	4,7 ± 0,6
A_0 (F)	(2,66 ± 0,07) · 10^{-3}	(2,01 ± 0,03) · 10^{-3}
γ	0,385 ± 0,006	0,376 ± 0,003

From GCD, the specific capacitance C_{SP} (F/g) was calculated from the total capacitance C of the supercapacitor:

$$C_{SP} = 4\frac{C}{m_{AM}}$$

where m_{AM} is the total mass of the active material. Specific energy E (Wh/kg) of the material in the supercapacitor is given by:

$$\boldsymbol{E = \frac{C\,U_{max}^2}{2\,m_{AM}\,3600}}$$

where U_{max} (V) is the maximum electrochemical stability region.

The maximum theoretical specific power P (kW/kg) that the material can supply is obtained by:

$$\boldsymbol{P = \frac{U_{max}^2}{4\,ESR\,m_{AM}}}$$

where ESR (Ω) is the equivalent series resistance of the supercapacitor. For each cycle, Coulombic efficiency has been calculated as:

$$\eta_C = \frac{C_D}{C_C}$$

where C_D and C_C are, respectively, the discharge and charge capacity for a given cycle (*Adv. Mater.* 2014, **26**, 2219–2251).

8. Green chemistry metrics evaluation

The green chemistry metrics reported in Table S10 have been evaluated through the guideline proposed by Fantozzi *et al* (*Chem. Soc. Rev.* 2023, **52**, 6680).

Table S10. Comparison of green chemistry metrics between **Cu-HHTP(M)** and **Cu-HHTP(S)** synthetic processes.

	M	S	Optimal Value
AE	78.9	78.9	100
RAE	0.27	0.0085	1
E-Factor	1197	1221	0
PMI	3.75	117	1
RME	53.3	44.6	100
MI	2.82	15.9	1
MP	35.5	6.26	100
Mol. E	0.025	0.0004	1

AE: atom economy; RAE: real atom economy; E-Factor: environmental factor; PMI: process mass intensity; RME: reaction mass efficiency; MI: mass intensity; MP: mass productivity; Mol. E: molar efficiency

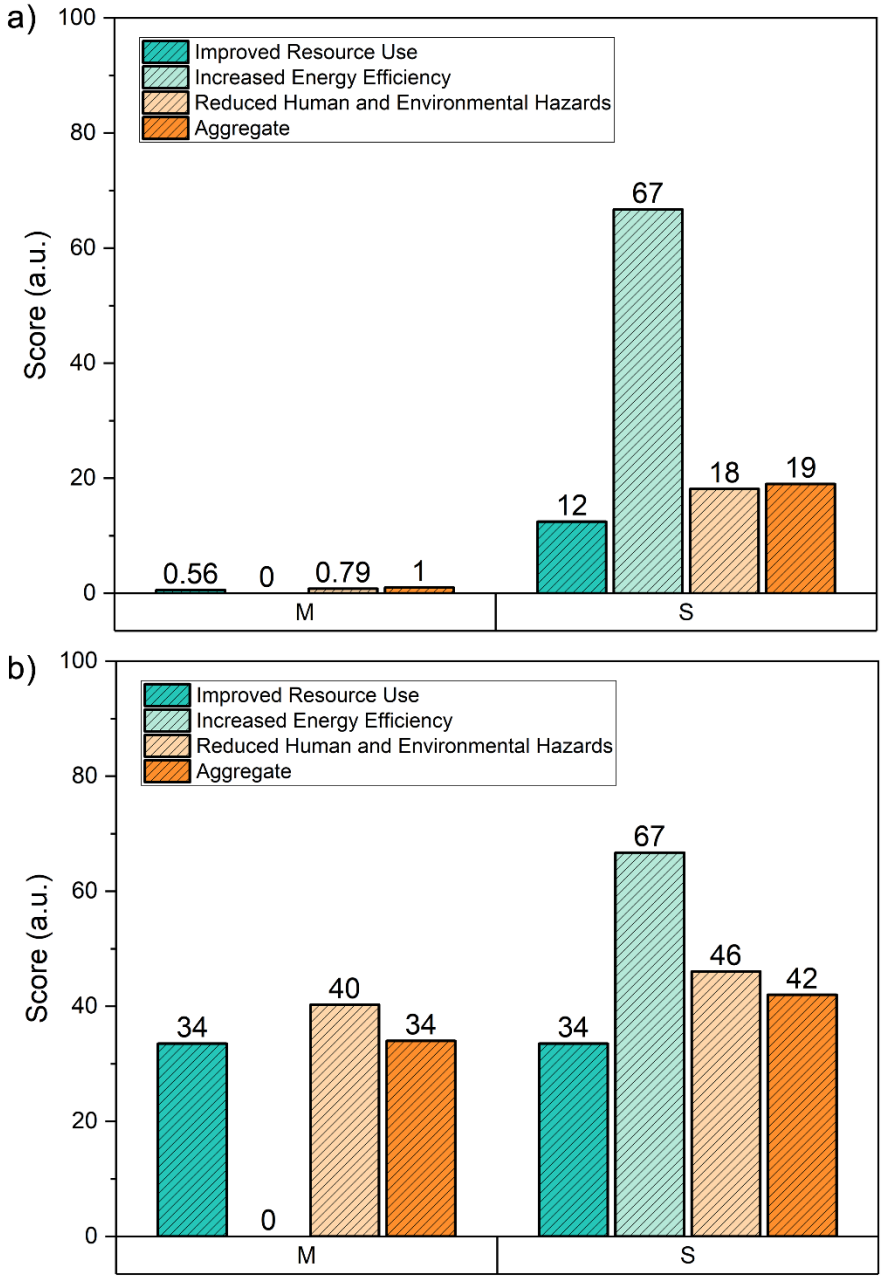

Fig. S29. Comparison of the greenness score, obtained from the assessment of product greenness conducted through DOZN 2.0 tool (*J. Chem. Educ.* 2021, **98**, 84-91), for **Cu-HHTP(M)** and **Cu-HHTP(S)** taking into account just the reaction process (a) and considering the work-up process (b).